Universal Maximum Strength of Solid Metals and Alloys

Duane D. Johnson,[1,2,*,†] Prashant Singh,[2] A. V. Smirnov,[2] and Nicolas Argibay[2]
[1]Department of Materials Science and Engineering, Iowa State University, Ames, Iowa 50011, USA
[2]Ames Laboratory, U.S. Department of Energy, Iowa State University, Ames, Iowa 50011, USA

(Received 2 September 2022; revised 19 February 2023; accepted 16 March 2023; published 19 April 2023)

Interstitial electron density ρ_o is offered as a direct metric for maximum strength in metals, arising from universal properties derived from an electron gas. ρ_o sets the exchange-correlation parameter r_s in density-functional theory. It holds also for maximum shear strength $\tau_{\max}$ in polycrystals [M. Chandross and N. Argibay, Phys. Rev. Lett. **124**, 125501 (2020)]. Elastic moduli and $\tau_{\max}$ for polycrystalline (amorphous) metals are linear with ρ_o and melting T_m (glass-transition T_g) temperature. ρ_o or r_s, even with rule-of-mixture estimate, predicts relative strength for rapid, reliable selection of high-strength alloys with ductility, as confirmed for elements to steels to complex solid solutions, and validated experimentally.

DOI: 10.1103/PhysRevLett.130.166101

With rising interest in design of increasingly complex metallic systems, it is critical to deliver fast and reliable physics-based metrics for materials optimization. An approach that links bond strength and strength of metals, and provides fast prediction (without adjustable parameters), remains elusive. A simple metric would facilitate accelerated design of reliable and damage-tolerant, high-strength metallic alloys for high-temperature applications (e.g., higher efficiency energy generation), including multi-principal-element alloys (MPEAs) [1–5], an exciting class of materials with a vast design space and emerging unique properties [6–10]. Metals are limited by their operational temperature and strength.

With perspective from Gilman [11,12] on response of materials to applied stress, we offer a simple, unifying, physics-based metric that provides quantitatively correct results to accelerate design that is computationally less burdensome and requires little *a priori* knowledge. For example, bulk modulus (B) reflects volumetric response to hydrostatic stress and data on ionic materials show $B \sim r_o^{-4}$ [11] (r_o is interatomic spacing), justified by potentials dominated by a Coulomb interaction. Nevertheless, it is surprising that alkali metals and tetrahedrally covalently bonded crystals and cubic-diamond compounds also exhibit this behavior, while mixed primary-bonded transition-metal carbides do not. For crystalline metals and ionic compounds, Gilman also provided a fairly accurate model for surface energy from Young's moduli (E) and atomic radii, effectively a measure of average bond strength in uniaxial tension [13].

Since Frenkel's work [14], estimates of shear strength based on shear moduli G [15] give maximum shear strength as $\tau_{\max} \approx G/30$, an order-of-magnitude estimate—a factor of 1000 too large for dislocation-mediated cases. Using density-functional theory (DFT), ideal (dislocation-free) maximum tensile strength estimated from changes of energy per atom along an ideal Bain path [16,17] gives 10–100 GPa, a factor of 100 too large. With defects, DFT can be quantitative, e.g., twinning stresses [18,19] and stacking-fault energies [20], but require large supercells that are computationally costly. Some bcc metals have variable strength or ductility due to electronic effects [21].

An estimate of E, associated with bond strength (stiffness), is found using scaling (in SI units [15]), i.e.,

$$E \approxeq 100 \frac{k_B T_m}{V_{\text{atom}}} \left[1 - 0.5 \frac{T}{T_m}\right] \text{GPa} \xrightarrow{T=0} 100 \frac{k_B T_m}{V_{\text{atom}}}. \quad (1)$$

(T_m) T is (melting) temperature in Kelvin and V_{atom} is volume per atom (in Å). At 0 K, Eq. (1) is fairly accurate (see Supplemental Material [22] Fig. S1). In isotropic polycrystals with Poisson's ratio ν, $B = E[3(1-2\nu)]^{-1}$ and $G = E[2(1+\nu)]^{-1}$ will also scale with T_m, giving similar relative elastic strength. Chandross and Argibay [23] recently argued a maximum achievable $\tau_{\max}$ in a polycrystalline metal (including grain- or sample-size effects) is given by [similar to Eq. (1) as $L \propto k_B T_m$ (see Fig. S2)]

$$\tau_{\max} \approxeq \left(L \frac{\rho_L}{M}\right) \left[1 - \frac{T}{T_m}\right] f_g \text{ GPa} \xrightarrow{T=0} k_B T_m \left(\frac{\rho_L}{M}\right) f_g, \quad (2)$$

where $(L\rho_L/M)$ estimates the product of average bond strength and bond density from intrinsic properties L (molar heat of fusion), ρ_L (density of liquid at T_m), M (atomic mass). With d (δ) is grain diameter (grain-boundary width), $f_g = [(d-\delta)/d]^3$ is volume fraction of crystalline grains that incur amorphization energy penalty. With $f_g = 1$ (single crystal), Eq. (2) is a good upper bound to maximum strength [23].

We reveal strength measures (e.g., moduli and $\tau_{\max}$) in metals (Fig. 1) and alloys (Fig. 2), which are expensive to

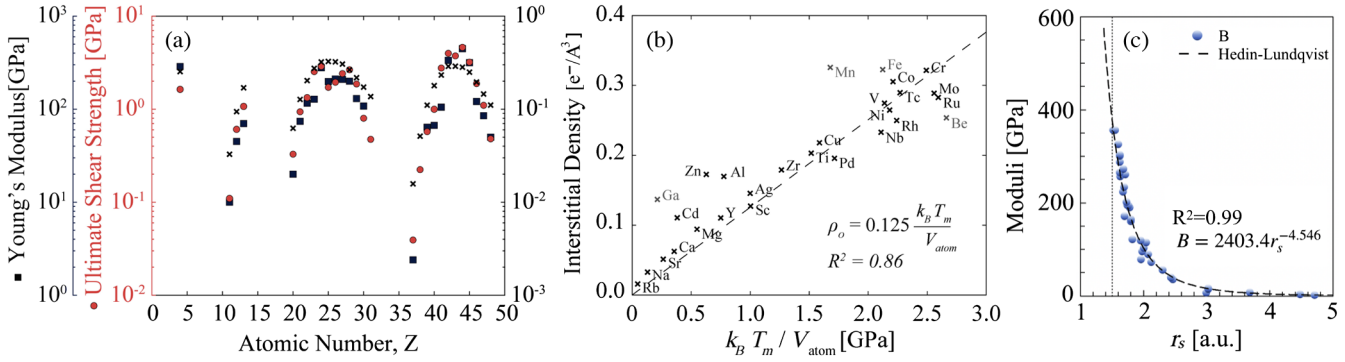

FIG. 1. (a) E (shaded square) and $\tau_{\max}$ (shaded circle) [GPa] (from [23]) vs Z; B is same [24]. On right vertical axis, DFT ρ_o (×) vs Z correlates with E, G, and B. (b) ρ_o vs $k_B T_m / V_{\text{atom}}$ shows linear correlation—R^2 is without outliers (Ga, Mn, Fe, Be) having allotropic transitions unaccounted in ρ_o. (c) Measured E, G, B vs r_s follow Hedin-Lundqvist electron-gas (dashed) curve. Figure S4 in Supplemental Material [22] compares all moduli and fits; deviations of E, G arise from Poisson's ratio (deformation anisotropy), where, for $\nu = 1/3$, $E = B$ but $G = (3/8)B$ follows the same curve that is lower (true for all ν).

compute or measure, correlate with an easily computed scalar—average interstitial electron density ρ_o. From properties of a homogeneous electron gas, ρ_o follows a DFT universal curve (scatter due to alloy stability changes). We show that ρ_o is linear with T_m (glass-transition temperature T_g) for crystalline (amorphous) metals. Thus, ρ_o is a fast relative strength measure for metals, including complex solid solutions and metallic glasses, as validated by measured data. We also find that a rule-of-mixtures (RoM) estimate from the elements provides a reliable ρ_o for an alloy, as confirmed by DFT and measured data. Supplemented with a RoM estimate of Pugh ratio (PR) assesses whether strength is potentially accompanied by ductility—critical for engineering applications. Our validated RoM ρ_o and PR permits accelerated alloy selection from only trivial computations.

Measures of strength are reflecting universal behavior and the physics is simple: with applied stress, atoms move closer together within a region containing only interstitial electrons, compressing the electron gas (homogeneous ρ_o in DFT). The larger ρ_o the larger the repulsion—the higher B (E) for hydrostatic (uniaxial) case. This correlation for B in elemental metals was shown by Moruzzi, Janak, and Williams [24] (not shown for clarity). See Supplemental Material [22] for comparison to full-potential linearized augmented plane [25] and for antiferromagnetic elements [26,27]. So, we focus on "universality" of ρ_o vs Z, and, except for scales, B [see fitted eq. in Fig. 1(c)], E (Eq. (1), and τ (Eq. (2) follow directly ρ_o vs Z [Fig. 1(a)]; for ρ_o of 10^{-1} $e/\text{Å}^3$, scales are 10^2 [10^0] for E [τ].

Typically, the interstitial around an atom is considered outside a nonoverlapping, inscribed sphere (IS) for a structure. The volumes of unit cell Ω_{cell} and IS Ω_{IS} are given by geometry (e.g., bcc) and lattice parameters $\{a_i\}$. For elements with Z [28] or solid solutions [29–33] with average $\bar{Z}$, the interstitial ρ_o (or charge Q_o) in interstitial volume $\Omega_o = \Omega_{\text{cell}} - \Omega_{\text{IS}}$ is

$$\rho_o \Omega_o = Q_o = \bar{Z} - \int_0^{\text{IS}} d\boldsymbol{r}\, \bar{\rho}(\boldsymbol{r}). \tag{3}$$

For muffin-tin potentials, the local exchange-correlation (xc) energy functional $\epsilon_{\text{xc}}[r_s]$ and potential $\mu_{\text{xc}}(r_s)$ is defined [24,34] by r_s, through ρ_o (with $\frac{4}{3}\pi r_s^3 \equiv 1/\rho_o$). Relative to interstitial reference energy $\mu_{\text{xc}}[\rho_o]$, potentials have an electrostatic Ewald term (Ewald energy) dependent linearly on ρ_o (ρ_o^2) [28–31]. For an alloy, the IS radius is determined by saddle points in the density that depends on environment. [32,33].

For a binary, E_{form} thus has a large contribution proportional to the square of the difference in ρ_o for the constituent metals [35], similarly for complex solid solutions [29–32]. Clearly, ρ_o vs Z and large differences in ρ_o between, say, transition and alkali metals, directly affect E_{form} or T_m. We confirm in Fig. 1(b) ρ_o vs $k_B T_m / V_{\text{atom}}$ behaves linearly. (While estimates of T_m are possible by more quantitative methods, e.g., [36], they are demanding.) Takeaway: moduli vs r_s in Fig. 1(c) (and Fig. S4) follows universal curve and relative maximum strength is indicated by r_s (reflecting $r_s \to \rho_o \propto T_m$, B, E, or $\tau_{\max}$).

For metals, compounds, and complex solid solutions, we use DFT-based Green's function Korringa-Kohn-Rostoker (KKR) combined with the coherent-potential approximation (CPA) to get configurationally averaged properties for arbitrary random alloys [29–33,37], including for design [8,20] and chemically or vacancy-mediated ordering [38–40]. Because of averaging, KKR-CPA has only 1 (2) atom per cell for fcc and bcc (hcp) phases to get $\bar{\rho}(\boldsymbol{r})$ and find ρ_o via Eq. (3). For the Green's functions, we used a $L_{\max} = 3$ spherical harmonic basis (s, p, d, f symmetries) and semicircular contour integration with 24 complex energies, and Brillouin-zone (BZ) mesh [41] of $18 \times 18 \times 18$ for bcc and fcc ($16 \times 16 \times 10$ for hcp). For pure metals or ordered compounds, KKR and full-potential results agree well [32,33]. Our KKR-CPA package uses

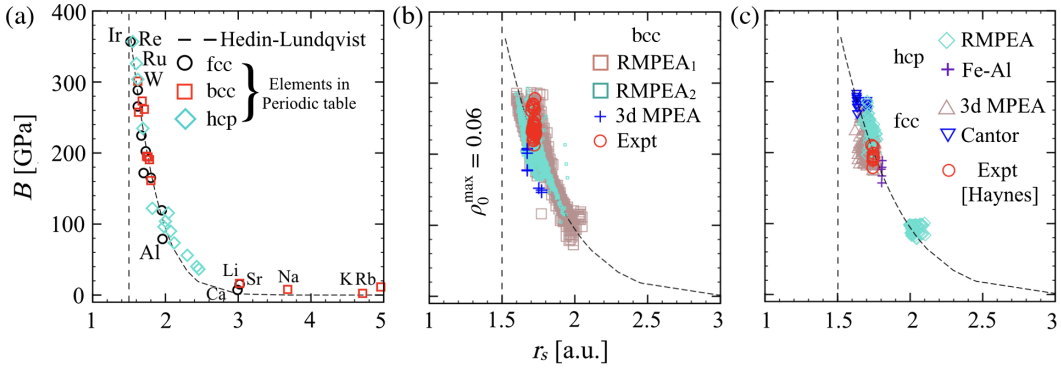

FIG. 2. From KKR (CPA), (a) bulk moduli B [GPa] vs r_s [a.u.] for a homogeneous electron gas ($[\frac{4}{3}\pi r_s^3]^{-1} = \rho_o$). (b) As in (a) but for bcc refractory (R)MPEAs and 3d MPEA, with example measured values. (c) As in (a) or (b) but for fcc- and hcp-MPEAs, compared to measured Haynes 282 steel values. For Hedin-Lundquist DFT functional (dashed lines), ρ_o values yield B values from the universal behavior. At $r_s \approx 1.5$, a maximum $\rho_o \approx 0.06\ e^-/\text{Å}^3$ yields maximum elemental B.

exchange-correlation functionals via LibXC [42], here done with Perdew-Burke-Ernzerhof (PBE) functional revised for solids [43,44] or Hedin-Lundqvist [34]. For Pugh ratio in MPEAs, we used supercell random approximates (SCRAPs) [45] with 60 ($5 \times 3 \times 2$) and 90 ($5 \times 3 \times 3$) atoms to mimic bcc random alloys (no short-range order to 3 neighbor shells). SCRAPs results were from VASP [46] with projector-augmented waves, [47,48] PBE functional [44], and 520 eV cutoff for plane-wave basis. BZ meshes [41] were $2 \times 5 \times 7$ (60 atom) and $2 \times 5 \times 5$ (90 atom). Convergence thresholds were 10^{-5} eV (0.01 eV/Å) for energy (forces). KKR-CPA and SCRAPs average a, E_{form}, and B agree [45]. For bcc-MPEAs, a fully relaxed SCRAP with local lattice distortions has ρ_o closer to CPA value (see Supplemental Material [22] for results and discussion).

Notably, as for elemental metals [Fig. 2(a)] with strength in correct measured order (here B) with Ir and Re at peak, solid-solution alloy results calculated (over 2800) follow the *universal electron-gas curve*; see Fig. 2(b) for bcc and Fig. 2(c) for fcc and hcp phases, including Cantor-type [1,5] alloys. Some scatter in the data is found along the curve as the alloys have crystal structure (an electron gas does not), and alloys near the curve are more stable (lowest E_{form}, and higher B), while less stable ones fall below the curve (lower B; see Fig. S5 and discussion). As such, a "vertical" behavior is found within alloy families vs composition as stability change (Fig. S5). Hence, r_s (ρ_o) provides a correct relative measure of B, E, G, τ, or T_m—but, in contrast to r_s, they are expensive to calculate or time-consuming to measure. $\rho_0^{\max}(r_s \approx 1.5)$ governs maximum strength (Fig. 2).

To validate correlations further, we compare measured B data [49] and the universal metric reflected in B vs r_s; see Fig. 2(b) for bcc-MPEAs (Mo-W-Ta-Ti-Ze-Cr/Al) and Fig. 2(c) for steels (Haynes-282). Measured data follows the universal r_s curve [again with caveat: most-stable alloys straddle the curve (Fig. S5) and less-stable are below it] and, hence, r_s serves as a relative measure of strength (stability): a smaller r_s has higher strength. Of course, in addition to strength, decreasing grain size (Hall-Petch behavior) can increase yield and ultimate-tensile strength [50]; tuning chemistry can strengthen via twinning- or transformation-induced plasticity [7,20]; or multiphase MPEA superalloys can show high specific strength [51].

For practicality in most technological applications, metals should have high strength and ductility, as needed to avoid brittle behavior and premature failure. Ideally, then, strength combined with a metric to assess ductility quickly for any complex alloy is desired. For MPEAs, we find surprising results involving Pugh's ratio (PR $= B/G$) [52], which captures for crystalline cases the extent of the plastic range without fracture, reflecting competition between resistance to plastic deformation (G) and fracture strength (B). PR $\gtrsim 1.8$ indicates ductility, brittle below this. For isotropic polycrystalline metals, PR depends only on ν, i.e., $B/G \to [2(1+\nu)/3(1-2\nu)]$. For simplicity, we tested for MPEAs compositionally weighted (c_i) elemental RoM with

$$\text{PR} = \frac{2(1+\bar{\nu})}{3(1-2\bar{\nu})}, \quad \text{and} \quad \bar{\nu} = \sum_{i=1}^{N} c_i \nu_i. \tag{4}$$

In Fig. 3, DFT PR vs Eq. (4) for 300 MPEAs agree, as verified experimentally [49]. A higher ρ_o indicates higher B and metallic properties. For Cr-rich MPEAs, Pugh ratio fails to predict the observed ductile-to-brittle crossover; nevertheless the linear behavior remains.

We now turn to bulk-metallic glasses (BMGs) or amorphous metals. To assess ρ_o and evaluate, among other quantities, the shear moduli G, we require supercells with densities (volumes) mimicking the high-temperature, non-crystalline metal (left for future work). However, as with crystalline metals, we anticipate that ρ_o for amorphous metals will show similar linear behavior with G and $k_B T_g / V_{\text{atom}}$. Note that T_g, as often reported, is a surrogate for Kauzmann temperature in limit of infinite heating rate.

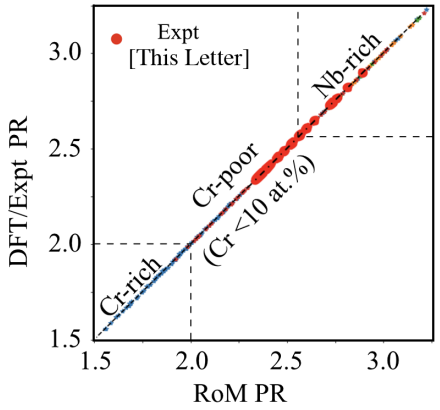

FIG. 3. Using SCRAPs, DFT Pugh Ratio (PR) vs Eq. (4), along with measured data (red circles [49]) for 32 alloys with compositions $(\text{Mo-W})_{1-x-y}(\text{Ti-Zr})_x\text{Ta}_y$. DFT data are for 300 W-Mo-Nb-Ta-Ti-Cr-Al alloys, varying mainly Cr and Nb content.

Hence, we plot $\tau_{\max}$ and $k_B T_g/V_{\text{atom}}$ vs G [Fig. 4(a)] using measured data for BMG [53–55] and amorphous MPEAs [56]. Indeed, both results mirror one another with linear correlation. So, we anticipate that ρ_o for amorphous metals follows the same r_s correlation. Indeed, we plot in Fig. 4(b) the measured $\tau_{\max}$ vs RoM-r_s [G differs by a scale from Fig. 4(a)], and they follow the r_s curve. For Vitreloy BMG [$Zr_{41.2}Ti_{13.8}Cu_{12.5}Ni_{10}Be_{22.5}$], from KKR-CPA in bcc phase with same volume and similar (14 atom) coordination number to BMG (15 atom) found experimentally [57], we find DFT-$r_s \sim 2\%$ larger than RoM-r_s value in Fig. 4(b) (likely due to using elemental ground-state crystalline values to estimate BMG phase). In Fig. 4(a), measured data below linear is likely due to heating rates or sample defects (e.g., inclusions, voids, and oxide), all of which are common, affecting τ or G due to limited ductility and dependence on quench rate [58].

Before concluding, we offer a "periodic table" for elements in hcp, fcc, and bcc phases and associated B and ρ_o (Supplemental Material [22], Fig. S6). Within an elemental group, ρ_o (or r_s) should be similar, yielding a similar B; in fact, for atoms in elemental period 2–6, the correlation coefficient is $C(\rho_0, B) \geq 0.95$. The stable phase and its lattice parameters dictate interstitial electron count, and influence the outcome of lowest phase. In Fig. S6, r_s gives the trend in B and takes a minimum at Group VIII, where bcc → hcp → fcc occurs. Notably, for MPEAs at zero pressure, we find good ρ_o or r_s values via RoM from values in Fig. S6 compared to direct DFT results [Fig. 5(a)]. From experiments on bcc-MPEAs [59], we confirm E vs RoM-r_s follows the universal curve [Fig. 5(b)]—again, scatter is from variation with composition (Fig. S5). As values overlay in Fig. 5(b), RoM-r_s is a reliable *a priori* estimate of DFT-r_s, i.e., strength by RoM from, e.g., $B[r_s] = 2403.4 r_s^{-4.546}$ GPa should mirror DFT results. Indeed, RoM-derived compositions for high strength fairly coincide with DFT down-selections that were validated by measurements on refractory MPEAs for high-T applications [49]; the same DFT-guided methods aided and accelerated development of high specific strength MPEA superalloys [51]. So, in alloys studied thus far, *a priori* RoM-ρ_o estimates could have more quickly narrowed regions with high strength.

Summary.—For single and polycrystalline metals, we have shown direct correlation between elastic moduli, tensile and shear strengths, and heat of fusion, all of which correlate with properties of an electron gas versus exchange-correlation $r_s[\rho_o]$ parameter—a *universal curve*. This behavior reflects the correlation of ρ_o vs Z (atomic number) or linear correlation with T_m (Figs. 1 and 2). Mechanical measures of strength also scale linearly with T_m and ρ_o. But, r_s can quickly assess relative strength in DFT, as confirmed experimentally (Fig. 2). A similar correlation with ρ_o is expected in amorphous metals, as suggested by measured data, where τ scales with G and T_g (Fig. 4). Finally, a rule-of-mixture r_s gives a fast *a priori* estimate strength of MPEA (Fig. 5) or BMGs (Fig. 4) to

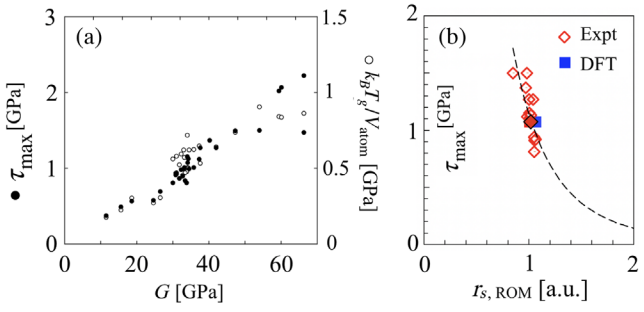

FIG. 4. For BMGs, we compare measured (a) $\tau_{\max}$ or $k_B T_g/V_{\text{atom}}$ vs G for 32 BMGs (tables in [53,56]), and (b) $\tau_{\max}$ vs RoM-r_s for 12 BMGs (table in [55]). In (a), $\tau_{\max}$ and T_g show identical linearity with G, differing by a scaling constant. PR above 1.8 [53]. For Vitreloy, KKR-CPA DFT-r_s [blue square] agrees to ~2% of RoM-r_s [solid diamond].

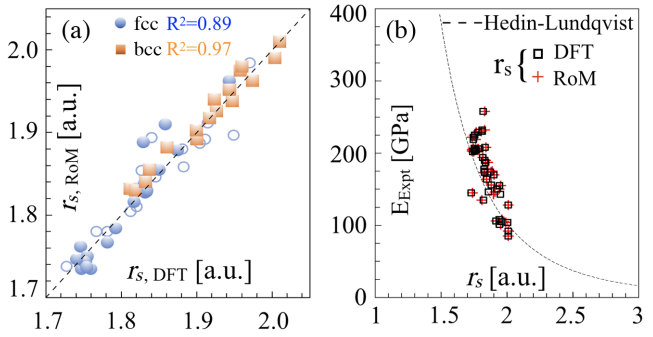

FIG. 5. (a) RoM r_s vs DFT r_s (R^2 from 1:1). RoM r_s uses values in Fig. S6 ("periodic table" for elements). Outlier data (off 1:1 line) is for magnetic fcc-MPEAs. (b) For clarity, bcc-MPEA measured [59] E vs r_s from DFT (squares) and RoM (pluses), relative to universal electron-gas curve.

accelerate design, e.g., for high-temperature strength and ductility (Fig. 3) or to train machine-learning models using a physics-based feature.

Support for theory was from the U.S. Department of Energy (DOE), Office of Science, Basic Energy Sciences, Materials Science and Engineering Division. Ames National Laboratory is operated by Iowa State University for the DOE under Contract DE-AC02-07CH11358. Theory-guided experiment for accelerated design of refractory MPEAs (with G. Ouyang and J. Cui) was supported by the Office of Energy Efficiency and Renewable Energy, Advanced Manufacturing Office under AOP 2.1.0.19; with advances on MPEA hardness (N. A.) under AOP 2.1.0.11.

*Corresponding author.
ddj@iastate.edu
†ddj@ameslab.gov

[1] B. Cantor, I. Chang, P. Knight, and A. Vincent, Mater. Sci. Eng. A **375**, 213 (2004).
[2] J.-W. Yeh, S.-K. Chen, S.-J. Lin, J.-Y. Gan, T.-S. Chin, T.-T. Shun, C.-H. Tsau, and S.-Y. Chang, Adv. Eng. Mater. **6**, 299 (2004).
[3] D. Miracle and O. Senkov, Acta Mater. **122**, 448 (2017).
[4] E. P. George, D. Raabe, and R. O. Ritchie, Nat. Rev. Mater. **4**, 515 (2019).
[5] B. Cantor, Prog. Mater. Sci. **120**, 100754 (2021).
[6] Y. T. Zhu and X. Liao, Nat. Mater. **3**, 351 (2004).
[7] Z. Li, K. G. Pradeep, Y. Deng, D. Raabe, and C. C. Tasan, Nature (London) **534**, 227 (2016).
[8] P. Singh, A. Sharma, A. V. Smirnov, M. S. Diallo, P. K. Ray, G. Balasubramanian, and D. D. Johnson, npj Comput. Mater. **4**, 16 (2018).
[9] Y. Ikeda, I. Tanaka, J. Neugebauer, and F. Körmann, Mater. Charact. **147**, 464 (2019).
[10] S. Picak, J. Liu, C. Hayrettin, W. Nasim, D. Canadinc, K. Xie, Y. Chumlyakov, I. Kireeva, and I. Karaman, Acta Mater. **181**, 555 (2019).
[11] J. J. Gilman, *Micromechanics of Flow in Solids* (McGraw-Hill, New York, 1969), Chap. 2, pp. 29–41.
[12] J. J. Gilman, *Electronic Basis of the Strength of Materials* (Cambridge University Press, New York, 2003).
[13] J. J. Gilman, J. Appl. Phys. **31**, 2208 (1960).
[14] J. Frenkel, Z. Phys. **37**, 572 (1926).
[15] T. H. Courtney, *Mechanical Behavior of Materials*, 2nd ed. (Waveland Press, Inc., Long Grove, IL, 2005).
[16] P. J. Craievich, M. Weinert, J. M. Sanchez, and R. E. Watson, Phys. Rev. Lett. **72**, 3076 (1994).
[17] M. Šob, L. Wang, and V. Vitek, Mater. Sci. Eng. A **234**, 1075 (1997).
[18] S. Kibey, J. Liu, D. Johnson, and H. Sehitoglu, Acta Mater. **55**, 6843 (2007).
[19] S. A. Kibey, L. L. Wang, J. B. Liu, H. T. Johnson, H. Sehitoglu, and D. D. Johnson, Phys. Rev. B **79**, 214202 (2009).
[20] P. Singh, S. Picak, A. Sharma, Y. I. Chumlyakov, R. Arroyave, I. Karaman, and D. D. Johnson, Phys. Rev. Lett. **127**, 115704 (2021).
[21] L. Qi and D. C. Chrzan, Phys. Rev. Lett. **112**, 115503 (2014).
[22] See Supplemental Material at http://link.aps.org/supplemental/10.1103/PhysRevLett.130.166101, with comparison for stability and strength.
[23] M. Chandross and N. Argibay, Phys. Rev. Lett. **124**, 125501 (2020).
[24] V. Moruzzi, J. Janak, and A. Williams, *Calculated Electronic Properties of Metals* (Pergamon Press, Inc., New York, 1978).
[25] K. Lejaeghere, V. V. Speybroeck, G. V. Oost, and S. Cottenier, Crit. Rev. Solid State Mater. Sci. **39**, 1 (2014).
[26] V. Moruzzi and P. Marcus, Phys. Rev. B **46**, 3171(R) (1992).
[27] D. Hobbs, J. Hafner, and D. Spisak, Phys. Rev. B **68**, 014407 (2003).
[28] J. F. Janak, Phys. Rev. B **9**, 3985 (1974).
[29] D. D. Johnson, D. M. Nicholson, F. J. Pinski, B. L. Gyorffy, and G. M. Stocks, Phys. Rev. Lett. **56**, 2088 (1986).
[30] D. D. Johnson, D. M. Nicholson, F. J. Pinski, B. L. Györffy, and G. M. Stocks, Phys. Rev. B **41**, 9701 (1990).
[31] D. D. Johnson and F. J. Pinski, Phys. Rev. B **48**, 11553 (1993).
[32] A. Alam and D. D. Johnson, Phys. Rev. B **80**, 125123 (2009).
[33] A. Alam and D. D. Johnson, Phys. Rev. B **85**, 144202 (2012).
[34] L. Hedin and B. I. Lundqvist, J. Phys. C **4**, 2064 (1971).
[35] A. Miedema, R. Boom, and F. De Boer, J. Less-Common Met. **41**, 283 (1975).
[36] Q.-J. Hong, J. Schroers, D. Hofmann, S. Curtarolo, M. Asta, and A. van de Walle, npj Comput. Mater. **7**, 1 (2021).
[37] A. Alam, B. Kraczek, and D. D. Johnson, Phys. Rev. B **82**, 024435 (2010).
[38] P. Singh, A. V. Smirnov, and D. D. Johnson, Phys. Rev. B **91**, 224204 (2015).
[39] P. Singh, A. Smirnov, A. Alam, and D. D. Johnson, Acta Mater. **189**, 248 (2020).
[40] P. Singh, S. Gupta, S. Thimmaiah, B. Thoeny, P. K. Ray, A. Smirnov, D. D. Johnson, and M. J. Kramer, Acta Mater. **194**, 540 (2020).
[41] H. J. Monkhorst and J. D. Pack, Phys. Rev. B **13**, 5188 (1976).
[42] M. A. Marques, M. J. Oliveira, and T. Burnus, Comput. Phys. Commun. **183**, 2272 (2012).
[43] J. P. Perdew, A. Ruzsinszky, G. I. Csonka, O. A. Vydrov, G. E. Scuseria, L. A. Constantin, X. Zhou, and K. Burke, Phys. Rev. Lett. **100**, 136406 (2008).
[44] J. P. Perdew, K. Burke, and M. Ernzerhof, Phys. Rev. Lett. **77**, 3865 (1996).
[45] R. Singh, A. Sharma, P. Singh, G. Balasubramanian, and D. D. Johnson, Nat. Comput. Sci. **1**, 54 (2021).
[46] G. Kresse and J. Furthmüller, Phys. Rev. B **54**, 11169 (1996).
[47] G. Kresse and D. Joubert, Phys. Rev. B **59**, 1758 (1999).
[48] P. E. Blöchl, O. Jepsen, and O. K. Andersen, Phys. Rev. B **49**, 16223 (1994).
[49] G. Ouyang, P. Singh, D. D. Johnson, M. J. Kramer, J. H. Perepezko, O. Senkov, D. Miracle, and J. Cui (to be published).
[50] Z. Li, C. C. Tasan, K. G. Pradeep, and D. Raabe, Acta Mater. **131**, 323 (2017).
[51] A. B. Kustas, M. R. Jones, F. W. DelRio, P. Lu, J. Pegues, P. Singh, A. Smirnov, J. Tiarks, E. D. Hintsala, D. D. Stauffer,

J. K. Román-Kustas, M. Abere, E. M. White, D. D. Johnson, I. E. Anderson, and N. Argibay, Appl. Mater. Today **29**, 101669 (2022).
[52] S. Pugh, London Edinburgh Dublin Philos. Mag. J. Sci. **45**, 823 (1954).
[53] W. L. Johnson and K. Samwer, Phys. Rev. Lett. **95**, 195501 (2005).
[54] Y. H. Liu, C. T. Liu, W. H. Wang, A. Inoue, T. Sakurai, and M. W. Chen, Phys. Rev. Lett. **103**, 065504 (2009).
[55] N. Argibay and M. Chandross, Phys. Rev. Mater. **6**, 115602 (2022).
[56] Y. Chen, Z.-W. Dai, and J.-Z. Jiang, J. Alloys Compd. **866**, 158852 (2021).
[57] C.-Y. Lee, Z. H. Stachurski, and T. Richard Welberry, Acta Mater. **58**, 615 (2010).
[58] C. A. Schuh, T. C. Hufnagel, and U. Ramamurty, Acta Mater. **55**, 4067 (2007).
[59] S. Gorsse, M. Nguyen, O. Senkov, and D. Miracle, Data Brief **21**, 2664 (2018).